

# Framing U-Net via Deep Convolutional Framelets: Application to Sparse-view CT

Yoseob Han and Jong Chul Ye\*, *Senior Member, IEEE*

**Abstract**—X-ray computed tomography (CT) using sparse projection views is often used to reduce the radiation dose. However, due to the insufficient projection views, a reconstruction approach using the filtered back projection (FBP) produces severe streaking artifacts. Recently, deep learning approaches using large receptive field neural networks such as U-net have demonstrated impressive performance for sparse view CT reconstruction. However, theoretical justification is still lacking. The main goal of this paper is, therefore, to develop a mathematical theory and to discuss how to improve these algorithms. In particular, inspired by the recent theory of *deep convolutional framelets*, we show that the U-net relies on a sub-optimal non-local bases that overly emphasizes low frequency components. The discovery leads to a dual frame and a tight frame U-net architectures for effective recovery of directional image components.

**Index Terms**—Deep learning, U-Net, compressed sensing CT, convolutional neural network (CNN), convolutional framelets

## I. INTRODUCTION

In X-ray CT, due to the potential risk of radiation exposure, the main research thrust is to reduce the radiation dose. Among various approaches for low-dose CT, sparse-view CT is a recent proposal that lowers the radiation dose by reducing the number of projection views [1]. However, due to the insufficient projection views, the FBP algorithm generates severe streaking artifacts. Accordingly, researchers have investigated compressed sensing approaches [2] that minimize the total variation (TV) or other sparsity-inducing penalties under a data fidelity term [1]. These approaches are, however, computationally expensive due to the repeated applications of projection and back-projection during iterative update steps.

Recently, deep learning approaches have achieved tremendous success in various fields, such as classification [3], segmentation [4], denoising [5], super resolution [6], [7], etc. In CT applications, Kang et al [8] provided the first systematic study of deep convolutional neural network (CNN) for low-dose CT and showed that a deep CNN using directional wavelets is more efficient in removing low-dose related CT noises. This work was followed by many extensions [9], [10], [11], [12]. Unlike these low-dose artifacts from reduced tube currents, the streaking artifacts originated from sparse projection views show globalized artifacts that are difficult to remove using conventional denoising CNNs [13], [14],

[15]. To address this problem, Jin et al [16] and Han et al [17] independently proposed residual learning networks using U-Net [4]. Because the streaking artifacts are globally distributed, CNN architecture with large receptive field was shown essential in these works [16], [17].

Recently, our group proposed the theory called *deep convolutional framelets* as a powerful mathematical framework for deep CNNs in inverse problems [18]. The convolutional framelets was originally proposed by Yin et al [19] to generalize the low-rank Hankel matrix approaches [20], [21], [22] by representing a signal using a fixed non-local basis convolved with data-driven non-local basis. The novelty of our deep convolutional framelets is the discovery that encoder-decoder network structure emerges from the convolutional framelet expansion [18]. We further showed that the deep learning is indeed a nonlinear shrinkage operation applied to the deep convolutional framelet representation, and the neural network training problem is to learn the optimal local-bases from training data for a given non-local bases [18].

Inspired by the theory of deep convolutional framelets [18], here we show that the existing U-net architecture uses a redundant multi-resolution frame as non-local basis in order to obtain large receptive field; however, the recovery step is not optimal, since it overly emphasizes the low frequency component of the signal. An immediate consequence is blurring artifact. The discovery leads to two types of network architectures that overcome the limitations of U-net. First, we propose a *dual frame* U-net architecture to satisfy the signal recovery condition. However, the dual frame U-net is not optimal due to its relative large noise amplification factor. To address this, a *tight frame* U-net with orthogonal wavelet frame is also proposed. In particular, the tight frame U-net with Haar wavelet basis only requires additional high-frequency path to the existing U-net structure. To further improve the noise performance, we incorporate the signal boosting using concatenation to the tight-frame U-net. Our numerical experiments confirm that the dual frame and tight frame U-nets exhibits better high frequency recovery than the standard U-net in sparse view CT applications.

## II. MATHEMATICAL PRELIMINARIES

### A. Frame

A family of function  $\{\phi_k\}_{k \in \Gamma}$  in a Hilbert space  $H$  is called a *frame* if it satisfies the following inequality [23]:

$$\alpha \|f\|^2 \leq \sum_{k \in \Gamma} |\langle f, \phi_k \rangle|^2 \leq \beta \|f\|^2, \quad \forall f \in H, \quad (1)$$

Authors are with the Department of Bio and Brain Engineering, Korea Advanced Institute of Science and Technology (KAIST), Daejeon 34141, Republic of Korea (e-mail: {hanyoseob,jong.ye}@kaist.ac.kr).

Part of this work was presented in 2017 International Conference on Fully Three-Dimensional Image Reconstruction in Radiology and Nuclear Medicine.

where  $\alpha, \beta > 0$  are called the frame bounds. If  $\alpha = \beta$ , then the frame is said to be *tight*. A frame is associated with a *frame operator*  $\Phi$  composed of  $\phi_k$ :

$$\Phi = [\cdots \quad \phi_{k-1} \quad \phi_k \quad \cdots].$$

Then, (1) can be equivalently written by

$$\alpha \|f\|^2 \leq \|\Phi^\top f\|^2 \leq \beta \|f\|^2, \quad \forall f \in H,$$

and the frame bounds can be represented by

$$\alpha = \sigma_{\min}(\Phi\Phi^\top), \quad \beta = \sigma_{\max}(\Phi\Phi^\top),$$

where  $\sigma_{\min}(A)$  and  $\sigma_{\max}(A)$  denote the minimum and maximum singular values of  $A$ , respectively, and the superscript  $\top$  denotes the Hermitian transpose. When the frame lower bound  $\alpha$  is non-zero, then the recovery of the original signal can be done from the frame coefficient  $c = \Phi^\top f$  using the *dual frame*  $\tilde{\Phi}$  satisfying

$$\tilde{\Phi}\Phi^\top = I,$$

since  $\hat{f} = \tilde{\Phi}c = \tilde{\Phi}\Phi^\top f = f$ . The explicit form of the dual frame is given by the pseudo-inverse:

$$\tilde{\Phi} = (\Phi\Phi^\top)^{-1}\Phi. \quad (2)$$

If the frame coefficients are contaminated by the noise  $w$ , i.e.  $c = \Phi^\top f + w$ , then the recovered signal using the dual frame is given by

$$\hat{f} = \tilde{\Phi}c = \tilde{\Phi}(\Phi^\top f + w) = f + \tilde{\Phi}w.$$

Therefore, the *noise amplification factor* can be computed by

$$\frac{\|\tilde{\Phi}w\|^2}{\|w\|^2} = \frac{\sigma_{\max}(\Phi\Phi^\top)}{\sigma_{\min}(\Phi\Phi^\top)} = \frac{\beta}{\alpha} = \kappa(\Phi\Phi^\top),$$

where  $\kappa(\cdot)$  refers to the condition number. A tight frame has the minimum noise amplification factor due to  $\beta/\alpha = 1$ , and it is equivalent to

$$A^\top A = cI, \quad (3)$$

for some scalar  $c > 0$ .

## B. Hankel Matrix

Let  $f = [f[1], \dots, f[n]]^\top \in \mathbb{R}^n$  be the signal vector. Then, a wrap-around Hankel matrix  $\mathbb{H}_d(f)$  is defined by

$$\mathbb{H}_d(f) = \begin{bmatrix} f[1] & f[2] & \cdots & f[d] \\ f[2] & f[3] & \cdots & f[d+1] \\ \vdots & \vdots & \ddots & \vdots \\ f[n] & f[1] & \cdots & f[d-1] \end{bmatrix}$$

where  $d$  denotes the matrix pencil parameter. Hankel matrix is closely related to the convolution operations in CNN.<sup>1</sup> Specifically, for a given convolutional filter  $\psi = [\psi[1], \dots, \psi[d]]^\top \in \mathbb{R}^d$ , a single-input single-output (SISO) circular convolution can be represented using a Hankel matrix:

$$y = f \circledast \psi = \mathbb{H}_d(f)\psi \in \mathbb{R}^n. \quad (4)$$

<sup>1</sup>In this paper, to avoid special treatment of boundary condition, our theory is mainly derived using circular convolution.

Similarly, a single-input multi-output (SIMO) convolution using filter kernel  $\Psi = [\psi_1 \cdots, \psi_q] \in \mathbb{R}^{d \times q}$  can be represented by

$$Y = f \circledast \Psi = \mathbb{H}_d(f)\Psi \in \mathbb{R}^{n \times q} \quad (5)$$

where  $q$  denotes the number of output channels. A multi-input multi-output (MIMO) convolution is represented by

$$y_i = \sum_{j=1}^p f_j \circledast \psi_i^j, \quad i = 1, \dots, q \quad (6)$$

where  $p$  and  $q$  are the number of input and output channels, respectively;  $\psi_i^j \in \mathbb{R}^d, i = 1, \dots, q; j = 1, \dots, p$  refer to the corresponding filters with the filter length  $d$ . The corresponding matrix representation is then given by

$$Y = F \circledast \Psi = \mathbb{H}_{d|p}(F) \begin{bmatrix} \Psi_1 \\ \vdots \\ \Psi_p \end{bmatrix} \quad (7)$$

where

$$\Psi_j = [\psi_1^j \quad \cdots \quad \psi_q^j] \in \mathbb{R}^{d \times q}$$

and  $F := [f_1 \cdots f_p]$  and  $\mathbb{H}_{d|p}(F)$  is an *extended Hankel matrix* by stacking  $p$  Hankel matrices side by side:

$$\mathbb{H}_{d|p}(F) := [\mathbb{H}_d(f_1) \quad \mathbb{H}_d(f_2) \quad \cdots \quad \mathbb{H}_d(f_p)] \quad (8)$$

The multiple input single output (MISO) convolution is then a special case of MIMO convolution when the output channel dimension  $q = 1$ . The following Hankel matrix algebra from in [18] is useful for our analysis:

**Lemma 1.** [18] For  $f \in \mathbb{R}^n$  and  $\Psi, \tilde{\Psi} \in \mathbb{R}^{d \times q}$ ,

$$\mathbb{H}_d^\dagger(\mathbb{H}_d(f)\Psi\tilde{\Psi}^\top) = \frac{1}{d} \sum_{i=1}^q (f \circledast \psi_i \circledast \tilde{\psi}_i) \in \mathbb{R}^n. \quad (9)$$

## C. Deep Convolutional Framelets

The convolutional framelet by Yin et al [19] is a signal representation using two bases: local and non-local bases. More specifically, let  $\Phi$  and  $\tilde{\Phi} \in \mathbb{R}^{n \times m}$  (resp.  $\Psi$  and  $\tilde{\Psi} \in \mathbb{R}^{d \times q}$ ) are frame and its dual frame, respectively, such that

$$\tilde{\Phi}\Phi^\top = I_{n \times n}, \quad \Psi\tilde{\Psi}^\top = I_{d \times d}. \quad (10)$$

Then, for any  $n$ -dimensional vector  $f \in \mathbb{R}^n$ , Yin et al [19] showed the following convolutional framelet expansion:

$$f = \frac{1}{d} \sum_{i=1}^m \sum_{j=1}^q \langle f, \phi_i \circledast \psi_j \rangle \tilde{\phi}_i \circledast \tilde{\psi}_j \quad (11)$$

where  $\circledast$  denotes the circular convolution, and  $\phi_i$  and  $\psi_i$  denote the  $i$ -th column of  $\Phi$  and  $\Psi$ , respectively;  $\{\phi_i \circledast \psi_j\}$  and  $\{\tilde{\phi}_i \circledast \tilde{\psi}_j\}$  then constitute the frame bases and its dual, respectively. The condition (10) is essential to enable the exact decomposition in (11). Here, the column of the local basis  $\Psi$  and  $\tilde{\Psi}$  are often referred to as local filters and its dual filters. In addition,  $\Phi^\top$  is a non-local basis that further de-correlates the filtered signals by local filters  $\Psi$ .

They further showed that (11) has energy compaction when the underlying Hankel matrix has low dimensional structure; furthermore, for a fixed non-local bases  $\Phi$  and  $\tilde{\Phi}$ , the local bases  $\Psi$  and  $\tilde{\Psi}$  can be optimally learned from the data such that the framelet coefficients  $\langle f, \phi_i \otimes \psi_j \rangle$  can be sparsified. This allows image denoising by retaining small set of coefficients using shrinkage operation.

More specifically, consider an inverse problem that aims to obtain a noiseless signal  $f$  from a noisy measurement  $\tilde{f}$ :

$$\tilde{f} = f + e,$$

where  $e$  is the additive noise. The noisy input  $\tilde{f}$  is then represented using (11), whose framelets coefficients are given by  $\langle \tilde{f}, \phi_i \otimes \psi_j \rangle$ . Then, a denoising algorithm simply applies the nonlinear shrinkage operator  $\rho(\cdot)$  to the wavelet coefficients:

$$\hat{f} = \frac{1}{d} \sum_{i=1}^m \sum_{j=1}^q \rho \left( \langle \tilde{f}, \phi_i \otimes \psi_j \rangle \right) \tilde{\phi}_i \otimes \tilde{\psi}_j \quad (12)$$

This simple shrinkage is effective in removing artifacts especially when the framelet coefficients are sparse, and the main idea of [19] is to optimize the local basis with respect to the given non-local basis such that the convolutional framelets expansion has the most sparse representation.

By extending this idea significantly, in our companion paper [18] we showed that (11) comes from the Hankel matrix decomposition and the encoder-decoder layer structure of CNN emerges from (11). More specifically, using (10), we have

$$\begin{aligned} f &= \mathbb{H}_d^\dagger(\mathbb{H}_d(f)) = \mathbb{H}_d^\dagger(\tilde{\Phi} \Phi \mathbb{H}_d(f) \Psi \tilde{\Psi}^\top) \\ &= \mathbb{H}_d^\dagger(\tilde{\Phi} C \tilde{\Psi}^\top) \end{aligned} \quad (13)$$

where  $\mathbb{H}_d^\dagger(\cdot)$  is the generalized inverse of Hankel operator, and  $C$  is the framelet coefficient matrix obtained from a convolution:

$$C = \Phi^\top (\mathbb{H}_d(f) \Psi) = \Phi^\top (f \otimes \Psi). \quad (14)$$

We further showed that (13) can be equivalently represented by another convolution [18]:

$$f = (\tilde{\Phi} C) \otimes \tau(\tilde{\Psi}) \quad (15)$$

Here the two local filters in (15) and (14) are given by

$$\Psi := [\psi_1 \ \cdots \ \psi_q] \in \mathbb{R}^{d \times q}, \quad \tau(\tilde{\Psi}) := \frac{1}{d} \begin{bmatrix} \tilde{\psi}_1 \\ \vdots \\ \tilde{\psi}_q \end{bmatrix} \in \mathbb{R}^{dq}.$$

This implies that a CNN structure is emerged from the convolutional framelets. More specifically, if  $\Phi = I$ , then the structure in (15) and (14) is in fact equivalent to one layer of encoder-decoder network as shown in Fig. 1(a).

In order to obtain a multi-layered CNN structure, the convolutional framelet expansion should be extended for the multiple inputs, because a SIMO convolution generates the multiple outputs. More specifically, for a given matrix input  $Z \in \mathbb{R}^{n \times p}$ , the following convolutional framelet expansion can be obtained from the matrix decomposition of the extended

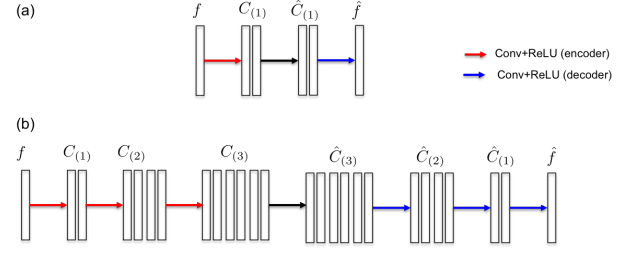


Fig. 1. (a) Single-layer encoder-decoder architecture, and (b) multi-layer encoder-decoder architecture.

Hankel matrix [18]:

$$Z = (\Phi C) \otimes \tau(\tilde{\Psi}) \quad (16)$$

where the framelet coefficients  $C$  is given by

$$C = \Phi^\top (Z \otimes \Psi) \quad (17)$$

Here, the encoder and decoder filters are defined by

$$\Psi := \begin{bmatrix} \psi_1^1 & \cdots & \psi_q^1 \\ \vdots & \ddots & \vdots \\ \psi_1^p & \cdots & \psi_q^p \end{bmatrix} \in \mathbb{R}^{dp \times q} \quad (18)$$

$$\tau(\tilde{\Psi}) := \frac{1}{d} \begin{bmatrix} \tilde{\psi}_1^1 & \cdots & \tilde{\psi}_q^1 \\ \vdots & \ddots & \vdots \\ \tilde{\psi}_1^p & \cdots & \tilde{\psi}_q^p \end{bmatrix} \in \mathbb{R}^{dq \times p} \quad (19)$$

and the convolution in (16) and (17) correspond to the multi-input multi-output (MIMO) convolution [18].

The simple convolutional framelet expansion using (15), (16), (14) and (17) is so powerful that the deep CNN architecture emerges from them. Specifically, by inserting the pair (17) and (16) between the pair (14) and (15), a deep CNN structure as shown in Fig. 1(b) can be interpreted as the multi-layered convolutional framelet expansion.

In general, the decoder structure of the  $l$ -layer implementation of a CNN can be mapped to the deep convolutional framelets as follows:

$$\begin{aligned} &g \left( C \left( \tilde{f}; \{\Psi^{(j)}\}_{j=1}^l \right); \{\tilde{\Psi}^{(j)}\}_{j=1}^l \right) \\ &= C \left( \tilde{f}; \{\Psi^{(j)}\}_{j=1}^l \right) \otimes \tau(\tilde{\Psi}^{(l)}) \otimes \tau(\tilde{\Psi}^{(l-1)}) \cdots \otimes \tau(\tilde{\Psi}^{(1)}) \end{aligned} \quad (20)$$

while the encoder layer of CNN for a given input  $\tilde{f}$  can be similarly mapped to:

$$C \left( \tilde{f}; \{\Psi^{(j)}\}_{j=1}^l \right) = \tilde{f} \otimes \Psi^{(1)} \otimes \Psi^{(2)} \cdots \otimes \Psi^{(l)}$$

Then, with the given input and target sample pairs  $\{\tilde{f}_i, f_i\}_{i=1}^N$  as training data, the  $L$ -layer convolutional framelets training problem is given by the estimation of the local bases:

$$\min_{\{\Psi^{(j)}, \tilde{\Psi}^{(j)}\}} \sum_{i=1}^N \left\| f_i - g \left( C \left( \tilde{f}_i; \{\Psi^{(j)}\}_{j=1}^L \right); \{\tilde{\Psi}^{(j)}\}_{j=1}^L \right) \right\|^2$$

where  $g(\cdot)$  is defined by (20) with rectified linear unit (ReLU) in appropriate locations. Now, the shrinkage behavior comes



cannot become a scaled identity matrix as in (3). Therefore, the U-Net frame is not tight and prone to noise boosting.

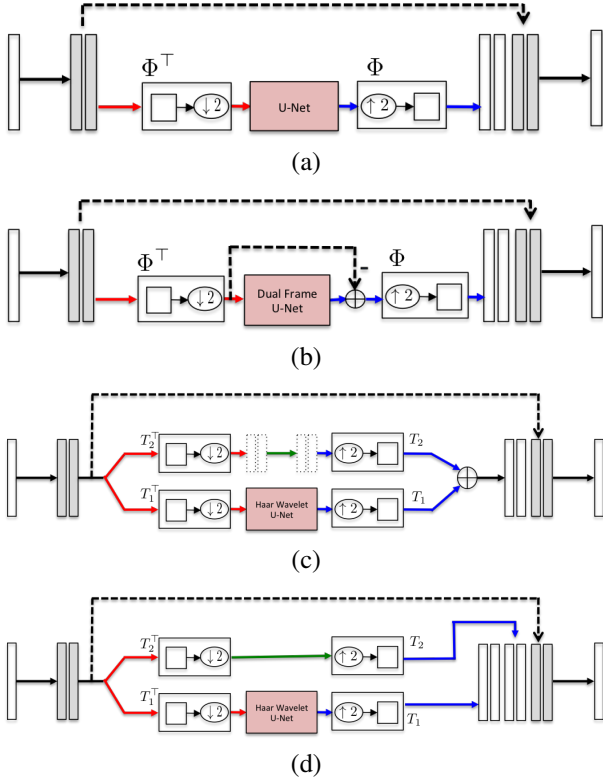


Fig. 5. Simplified U-net architecture and its variants. (a) Standard U-net, (b) dual frame U-net, (c) tight frame U-net using Haar wavelet, and (d) tight frame U-net with concatenation. Dashed lines refer to the skipped-connection, square-box within  $\Phi$ ,  $\Phi^\top$  and  $T_k$ ,  $T_k^\top$  correspond to the sub-band filters. The next level U-net units are recursively added to the low-frequency band signals.

Another important limitation of U-net is that it does not satisfy the recovery condition. While this can be readily seen from that U-net does not satisfy the condition (10), we can explicitly see this from the unique concatenation step in U-net (see Fig. 5(a)). More specifically, this step is given by

$$W = [f \otimes \Psi \quad P_{R(\Phi)}(f \otimes \Psi)] \quad (26)$$

where we use  $\Phi\Phi^\top = P_{R(\Phi)}$  for the case of average pooling. The final step of recovery is the MISO convolution, which is equivalent to taking pseudo-inverse of Hankel operator after multiplying dual local bases [18]:

$$\begin{aligned} \hat{f} &= \mathbb{H}_d^\dagger \left( W \begin{bmatrix} \Xi^\top \\ \Theta^\top \end{bmatrix} \right) \\ &= \mathbb{H}_d^\dagger (\mathbb{H}_d(f) \Psi \Xi^\top) + \mathbb{H}_d^\dagger (P_{R(\Phi)} \mathbb{H}_d(f) \Psi \Theta^\top) \\ &= \frac{1}{d} \sum_{i=1}^q (f \otimes \psi_i \otimes \xi_i + P_{R(\Phi)}(f \otimes \psi_i) \otimes \theta_i) \quad (27) \end{aligned}$$

where  $[\Xi \quad \Theta]$  denotes the local dual bases, and the last equality comes from (9) in Lemma 1. Note that the low frequency signal  $P_{R(\Phi)}(f \otimes \psi_i)$  is contained in both terms of (27); so it is overly emphasized, which is believed to be the main source of smoothing.

### C. Dual Frame U-Net

One simple fix for the aforementioned limitation is using the dual frame. Specifically, using (2), the dual frame for  $A$  in (25) can be obtained as follows:

$$\tilde{A} = (A^\top A)^{-1} A^\top = (I + \Phi\Phi^\top)^{-1} [I \quad \Phi] \quad (28)$$

Thanks to the the matrix inversion lemma and the orthogonality  $\Phi^\top\Phi = I$  for the case of average pooling, we have

$$\begin{aligned} (I + \Phi\Phi^\top)^{-1} &= I - \Phi(I + \Phi^\top\Phi)^{-1}\Phi^\top \\ &= I - \frac{1}{2}\Phi\Phi^\top \end{aligned}$$

Thus, the dual frame is given by

$$\begin{aligned} \tilde{A} &= (I - \Phi\Phi^\top/2) [I \quad \Phi] \\ &= [I - \Phi\Phi^\top/2 \quad \Phi/2] \quad (29) \end{aligned}$$

For a given framelet coefficients  $Y$  in (24), the reconstruction using the dual frame is then given by

$$\begin{aligned} \hat{C} &= \tilde{A}Y \quad (30) \\ &= \left( I - \frac{\Phi\Phi^\top}{2} \right) C + \frac{1}{2}\Phi S \\ &= C + \frac{1}{2} \underbrace{\Phi}_{\text{unpooling}} \underbrace{(S - \Phi^\top C)}_{\text{residual}} \quad (31) \end{aligned}$$

Now, Eq. (31) suggests a network structure for the dual frame U-Net. More specifically, unlike the U-net, the *residual signal* at the low resolution is upsampled through the unpooling layer. This can be easily implemented using additional by-pass connection for the low-resolution signal as shown in Fig. 5(b).

This simple fix makes the dual frame. Furthermore, the noise amplification factor for the dual frame U-net is the condition number of  $I + \Phi\Phi^\top = I + P_{R(\Phi)}$ , which is equal to 2. While this is twice bigger than the optimal one, it still provides a reasonable reconstruction performance.

Similar to the U-net, the final step of dual frame U-net is the concatenation and the MISO convolution, which is equivalent to applying  $\mathbb{H}_d^\dagger(\cdot)$  operation to the processed framelet coefficients multiplied with the local basis [18]. More specifically, the concatenated signal is given by

$$W = [C \quad \frac{1}{2}\Phi(S - \Phi^\top C)] \quad (32)$$

The final MISO convolution is equivalently computed by

$$\begin{aligned} \hat{f} &= \mathbb{H}_d^\dagger \left( W \begin{bmatrix} \Xi^\top \\ \Theta^\top \end{bmatrix} \right) \\ &= \mathbb{H}_d^\dagger (C \Xi^\top) + \frac{1}{2} \mathbb{H}_d^\dagger (\Phi S \Theta^\top) - \frac{1}{2} \mathbb{H}_d^\dagger (\Phi \Phi^\top C \Theta^\top) \\ &= \mathbb{H}_d^\dagger (\mathbb{H}_d(f) \Psi \Xi^\top) \\ &= \frac{1}{d} \sum_{i=1}^q (f \otimes \psi_i \otimes \xi_i) \quad (33) \end{aligned}$$

where the third equality comes from  $S = \Phi^\top C$ . Therefore, by choosing the dual local filter basis such that  $\Psi \Xi^\top = I$ , the right hand side of (33) becomes equal to  $f$ .

#### D. Tight Frame U-Net

Another way to improve the performance of U-net while maintaining the large receptive field is using tight filter-bank (FB) frames or wavelets. More specifically, instead of using pooling operation, the non-local transform  $\Phi^\top$  is now composed of (oversampled) filter bank:

$$\Phi = [T_1 \ \cdots \ T_L] \quad (34)$$

where  $T_k$  denotes the  $k$ -th subband operator. We further assume that the filter bank is tight, i.e.

$$\Phi\Phi^\top = \sum_{k=1}^L T_k T_k^\top = cI, \quad (35)$$

for some scalar  $c > 0$ . Then, the convolutional framelet coefficients including the by-pass connection can be written by

$$Y := A(f \circledast \Psi) = [C^\top \ S_1^\top \ \cdots \ S_L^\top]^\top \quad (36)$$

where

$$A := [I \ T_1 \ \cdots \ T_L]^\top, \quad C = f \circledast \Psi, \quad S_k = T_k^\top C.$$

Now, we can easily see that  $A$  is also a tight frame, since

$$A^\top A = I + \sum_{k=1}^L T_k T_k^\top = (c+1)I.$$

There are several important tight filter bank frames. One of the most simplest one is that Haar wavelet transform with low and high sub-band decomposition, where  $T_1$  is the low-pass subband, which is equivalent to the average pooling; and  $T_2$  is the high pass filtering given by

$$T_2 = \frac{1}{\sqrt{2}} \begin{bmatrix} 1 & -1 & 0 & 0 & \cdots & 0 & 0 \\ 0 & 0 & 1 & -1 & \cdots & 0 & \\ \vdots & & & & \ddots & \vdots & \\ 0 & 0 & 0 & 0 & \cdots & 1 & -1 \end{bmatrix}^\top$$

Then, we can easily see that

$$T_1 T_1^\top + T_2 T_2^\top = I$$

so the Haar wavelet frame is tight. The corresponding tight frame U-net structure is illustrated in Fig. 5(c). Note that compared to the standard U-net, there exists only additional high-pass branch, which is summed with low-pass signal. This simple fix makes the frame tight.

Aside from the noise robust recovery due to the minimum noise amplification factor, another important advantages of using wavelet tight frame as non-local bases is that the directional components can be processed using different convolutional filters shown as dotted boxes in Fig. 5(c). This may provide an opportunity to learn the directional components as demonstrated in [18]. However, this additional layers impose additional complexity to the network, so this paper only compares the networks without additional filters in the high pass layer. Another simple way to improve the performance is using concatenation. More specifically, rather than summing up the subband signals before concatenation, each subband

signal is by-passed to the individual concatenation layers as shown in as shown in Fig. 5(d). Then, rather than simple sum, the convolutional layer after the concatenation can provide weighted sum whose weights are learnt from data.

## IV. METHODS

### A. Data Set

As a training data, we used ten patient data provided by AAPM Low Dose CT Grand Challenge (<http://www.aapm.org/GrandChallenge/LowDoseCT/>). The data is composed of 3-D CT projection data from 2304 views. Artifact-free original images were generated by FBP using all 2304 projection views. Sparse view reconstruction input images were generated using FBP from 48, 64, 96, and 192 projection views, respectively. For our experiments, the label data were defined as the difference between the sparse view reconstruction and the full view reconstruction.

Among the ten patient data, eight patient data were used for training and one patient data was for validation, whereas the remaining one was used for test. This corresponds to 3602 slices of  $512 \times 512$  images for the training data, and 658 slices of  $512 \times 512$  images for the validation data. The test data was 488 slices of  $512 \times 512$  images. The training data was augmented by conducting horizontal and vertical flipping. For the training data set, we used the FBP reconstruction using 48, 96 and 192 projection views simultaneously as input and the difference between the full view (2304views) reconstruction and the sparse view reconstructions were used as label.

### B. Network Architecture

As shown in Fig. 3, the original, dual-frame and tight-frame U-nets consist of convolution layer, batch normalization [24], rectified linear unit (ReLU) [3], and contracting path connection with concatenation [4]. Specifically, each stage contains four sequential layers composed of convolution with  $3 \times 3$  kernels, batch normalization, and ReLU layers. Finally, the last stage has two sequential layers and the last layer contains only convolution layer with  $1 \times 1$  kernel. The number of channels for each convolution layer is illustrated in Fig. 3. Note that the number of channels are doubled after each pooling layers. The differences between the original, dual-frame and the tight-frame U-net are from the pooling and unpooling layers as shown in Figs. 5(a)-(d).

### C. Network training

The proposed network was trained by stochastic gradient descent (SGD). The regularization parameter was  $\lambda = 10^{-4}$ . The learning rate was set from  $10^{-3}$  to  $10^{-5}$  which was gradually reduced at each epoch. The number of epoch was 150. A mini-batch data using image patch was used, and the size of image patch was  $256 \times 256$ .

The network was implemented using MatConvNet toolbox (ver.24) [25] in MATLAB 2015a environment (Mathwork, Natick). We used a GTX 1080 Ti graphic processor and i7-7700 CPU (3.60GHz). The network takes about 1 day for training.

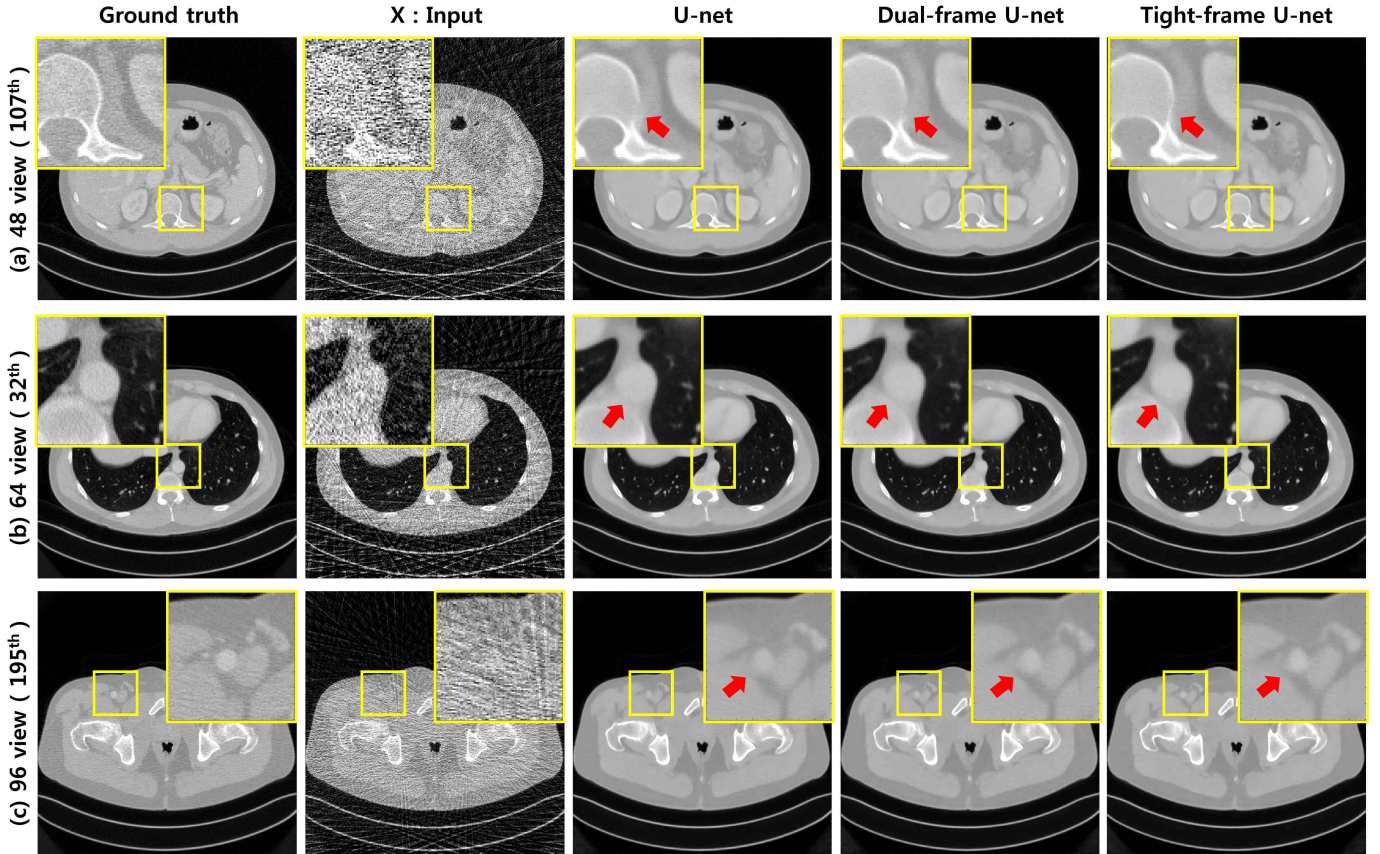


Fig. 6. Reconstruction results by original, dual-frame and tight frame U-nets at various sparse view reconstruction.

## V. EXPERIMENTAL RESULTS

Fig. 6 compare reconstruction results by original, dual-frame, and tight-frame U-nets. For the case of tight-frame U-net results, we use the tight frame U-net with concatenation (see Fig. 5(d)). All the methods provide impressive reconstruction performance. However, as shown in the magnified views, the original U-net provides a bit blurry edge images in many areas, whereas the dual-frame and tight-frame U-nets improved high frequency features of the images. Among the two tight frame U-net implementations in Fig. 5(c)(d), we observed that the advantages of the concatenation layer is more noticeable at sparser views. For example, as shown in Fig. 7, additional concatenation layer produces sharper edges at 48 views, whereas it provides nearly identical results in 64 views and higher. Moreover, while the NMSE values of various U-net implementation was about the same, the tight-frame U-net has exhibited consistently the best NMSE values across all downsampling factors. Specifically, the NMSE values of tight-frame U-net with the concatenation improved about 5~10% compared to the standard U-net across 48 and 384 views. Therefore, we use the tight-frame U-net with the concatenation in all the following experiments.

Fig. 8(a)-(c) compared the reconstruction results by the proposed method and TV from 48, and 96 projection views, respectively. Note that the same network was used for all these cases to verify the universality of the proposed method. The results in Fig. 8(a)-(c) clearly showed that the proposed

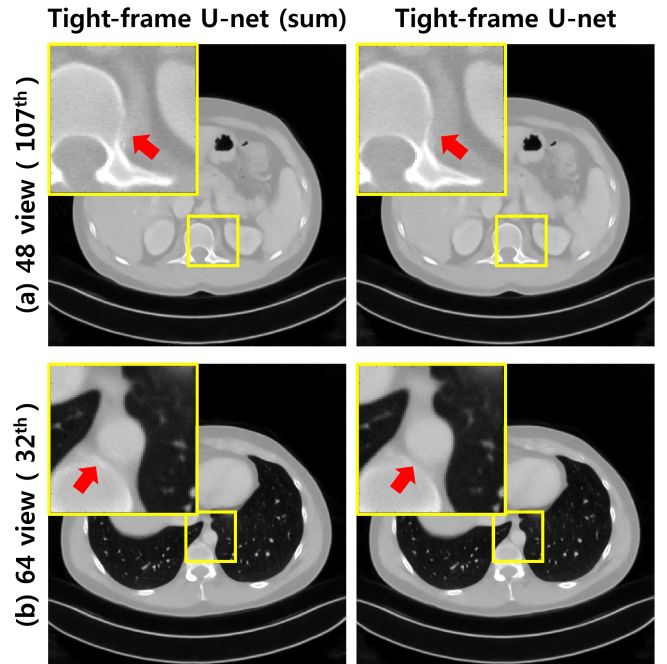


Fig. 7. Reconstruction results by two realizations of tight frame U-nets.

network removes most of streaking artifact patterns and preserves detailed structures of underlying images. The magnified view in Fig. 8(a)-(c) confirmed that the detailed structures

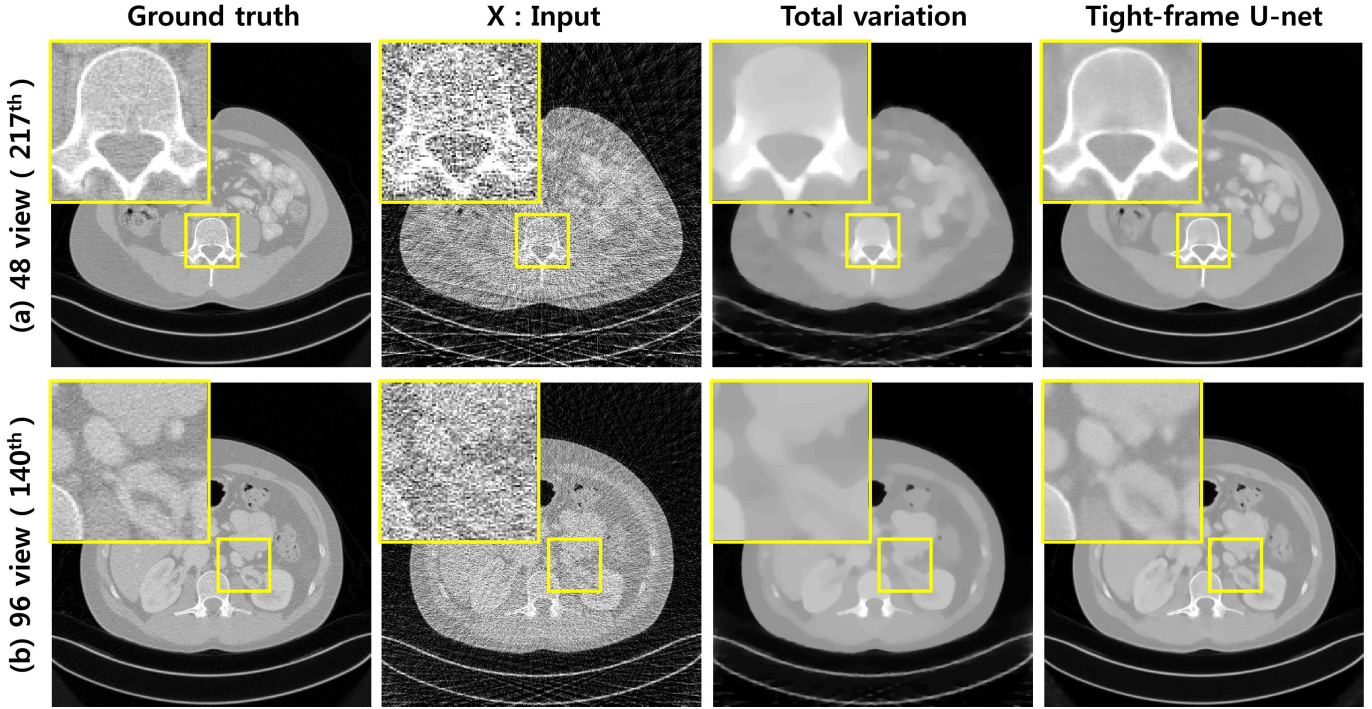


Fig. 8. Axial view reconstruction results by TV based compressed sensing and the proposed tight-frame U-net.

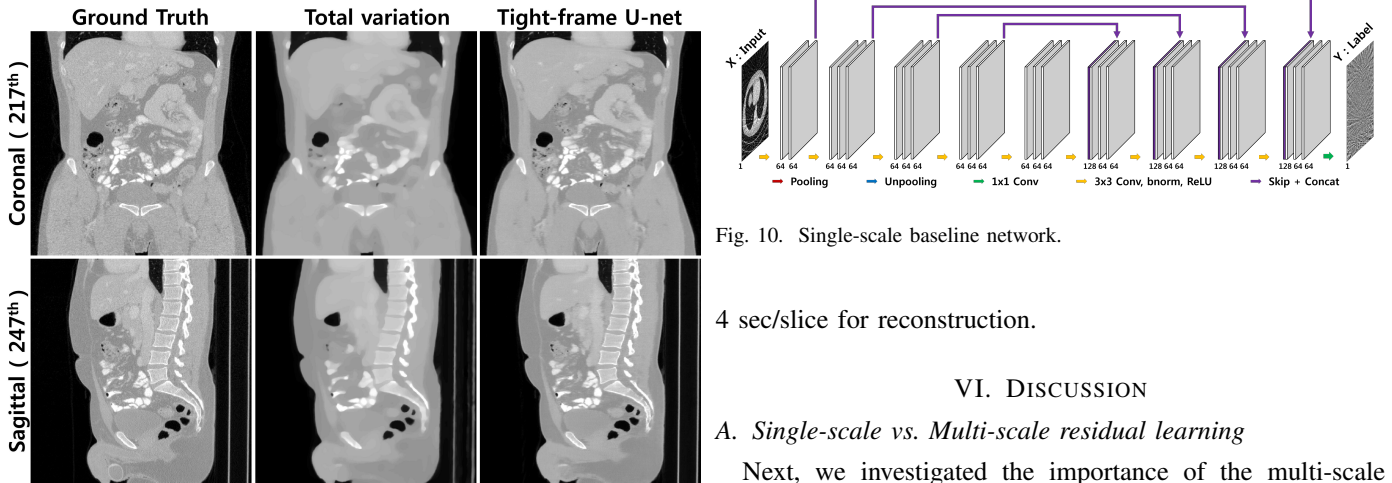


Fig. 10. Single-scale baseline network.

4 sec/slice for reconstruction.

## VI. DISCUSSION

### A. Single-scale vs. Multi-scale residual learning

Next, we investigated the importance of the multi-scale nature of residual learning using U-net. As for reference, a single-scale residual learning network as shown in Fig. 10 was used. Similar to the proposed method, the streaking artifact images were used as the labels. However, the residual network was constructed without pooling and unpooling layers. For fair comparison, we set the number of network parameters similar to the proposed method by fixing the number of channels at each layer across all the stages. In Fig. 11, the image reconstruction quality by the tight-frame U-net with concatenation was much improved compared to the single resolution one.

### B. Diversity of training set

Fig. 12 shows that reconstructed results by the tight-frame Unet, when the training data are composed of FBP images from (i) 48 views, (ii) 96 views, and (iii) 48, 96, and 192 views,

Fig. 9. Coronal and sagittal views of reconstruction results by TV based compressed sensing and the proposed tight-frame U-net.

are very well reconstructed using the proposed method. Fig. 9 shows reconstruction results using the tight-frame U-net from coronal and sagittal directions. Accurate reconstruction were obtained using the proposed method, whereas there exist severe blurring artifacts in TV reconstruction (or remaining streaking artifact if smaller regularization parameter was used). Moreover, compared to the standard compressed sensing CT approach with TV penalty, the proposed results in Fig. 8 and Fig. 9 provides significantly improved image reconstruction results, even though the computational time for the proposed method is 200 ms/slice. This is 18 time faster than the TV approach because the standard TV approach took about 3 ~



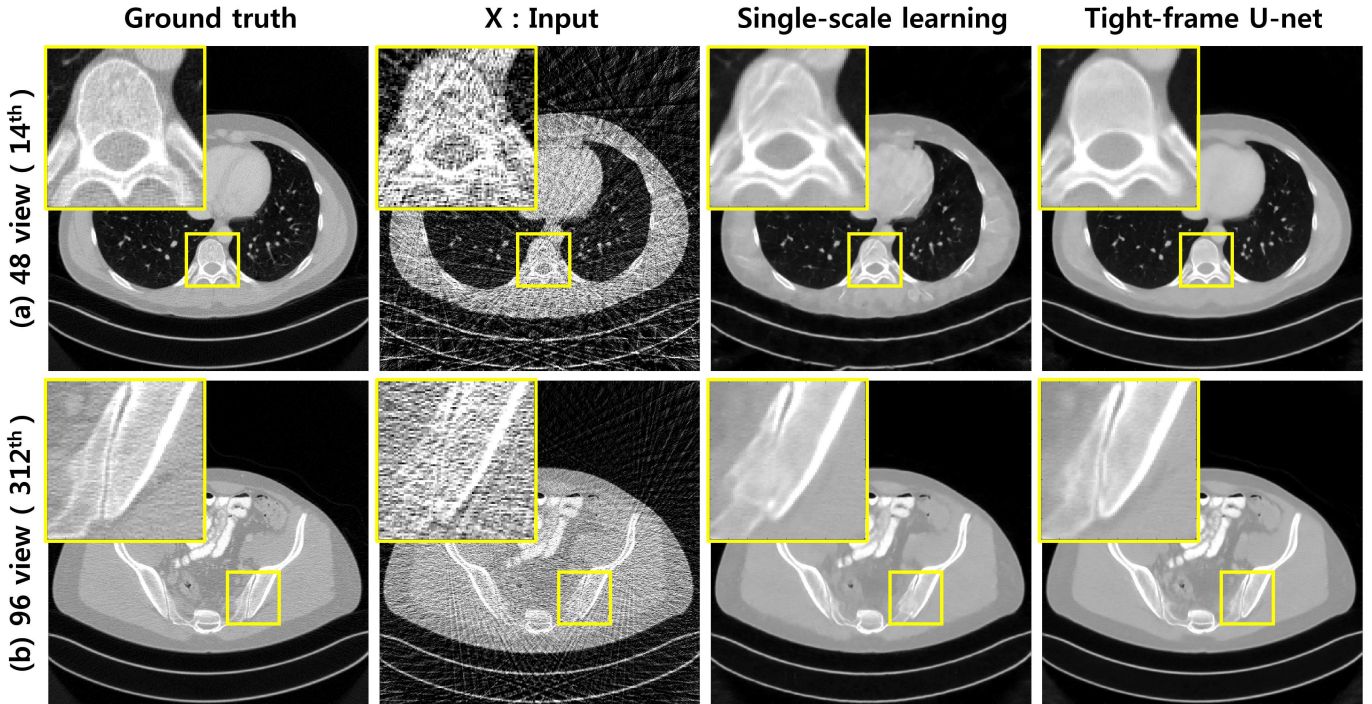


Fig. 11. Comparison results for single-scale versus multi-scale residual learning from 48 and 96 view reconstruction input data.

respectively. The streaking artifacts were removed very well in all cases; however, the detailed structure of underlying image was well-recovered for the case of (ii) 96 views and (iii) 48, 96, and 192 views cases; but the network trained with 48 views results in blurry reconstruction when it was applied to 192 view data (see Fig. 12(i)). On the other hand, when the network trained with only 96 views was applied to 48 views sparse CT reconstruction, the remaining streaking artifacts were visible as shown in Fig. 12(ii).

To make the network applicable across all ranges of view down-sampling, we therefore trained the network by simultaneously using FBP data from 48, 96, and 192 projection views. As shown in Fig. 12(iii), this combined training provided the best reconstruction across wide ranges of view down-sampling.

## VII. CONCLUSION

In this paper, we showed that large receptive field network architecture such as U-net is essential for sparse view CT reconstruction due to the globally distributed streaking artifacts. Based on the recent theory of deep convolutional framelets, we then showed that the existing U-net architecture does not satisfy the recovery condition due to the over-emphasis on the low-frequency signals and the resulting drawback is often manifested as the blurry and spurious image artifacts. In order to overcome the limitations, we proposed dual frame U-net and tight frame U-net. While the dual frame U-net was designed to satisfy the mathematically motivated recovery condition, the resulting modification was an intuitive additional skipped connection. For tight frame U-net with wavelets, additional path to process the subband signals were necessary. These additional path allows improved noise robustness and

directional information process that can be adapted to image statistics. Using extensive experiments, we showed that the proposed U-net variants were better than the conventional U-net for sparse view CT reconstruction.

## VIII. ACKNOWLEDGEMENT

The authors would like to thanks Dr. Cynthia MaCollough, the Mayo Clinic, the American Association of Physicists in Medicine (AAPM), and grant EB01705 and EB01785 from the National Institute of Biomedical Imaging and Bioengineering for providing the Low-Dose CT Grand Challenge data set. This work is supported by Korea Science and Engineering Foundation, Grant number NRF-2016R1A2B3008104.

## REFERENCES

- [1] E. Y. Sidky and X. Pan, "Image reconstruction in circular cone-beam computed tomography by constrained, total-variation minimization," *Physics in medicine and biology*, vol. 53, no. 17, p. 4777, 2008.
- [2] D. L. Donoho, "Compressed sensing," *IEEE Transactions on information theory*, vol. 52, no. 4, pp. 1289–1306, 2006.
- [3] A. Krizhevsky, I. Sutskever, and G. E. Hinton, "Imagenet classification with deep convolutional neural networks," in *Advances in neural information processing systems*, 2012, pp. 1097–1105.
- [4] O. Ronneberger, P. Fischer, and T. Brox, "U-net: Convolutional networks for biomedical image segmentation," in *International Conference on Medical Image Computing and Computer-Assisted Intervention*. Springer, 2015, pp. 234–241.
- [5] K. Zhang, W. Zuo, Y. Chen, D. Meng, and L. Zhang, "Beyond a gaussian denoiser: Residual learning of deep cnn for image denoising," *arXiv preprint arXiv:1608.03981*, 2016.
- [6] J. Kim, J. K. Lee, and K. M. Lee, "Accurate image super-resolution using very deep convolutional networks," *arXiv preprint arXiv:1511.04587*, 2015.
- [7] W. Shi, J. Caballero, F. Huszár, J. Totz, A. P. Aitken, R. Bishop, D. Rueckert, and Z. Wang, "Real-time single image and video super-resolution using an efficient sub-pixel convolutional neural network," in *Proceedings of the IEEE Conference on Computer Vision and Pattern Recognition*, 2016, pp. 1874–1883.

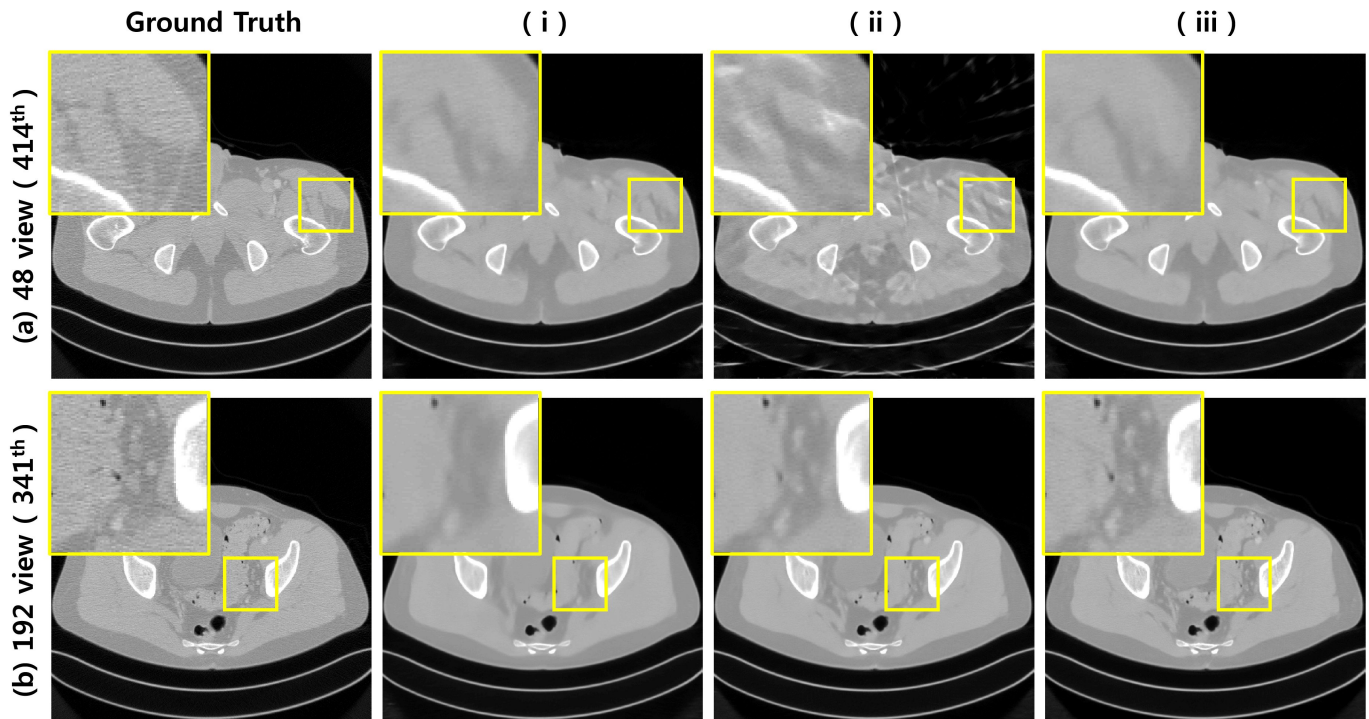


Fig. 12. Comparison results for various training data configuration. (Column direction) Reconstruction results by the tight-frame U-net trained using (i) 48 projection views, (ii) 96 projection views, and (iii) 48, 96, and 192 projection views, respectively. (Row direction) Reconstruction results by the tight-frame U-net when the trained network was applied to (a) 48 view test data, and (b) 192 view test data, respectively.

- [8] E. Kang, J. Min, and J. C. Ye, "A deep convolutional neural network using directional wavelets for low-dose x-ray CT reconstruction," *arXiv preprint arXiv:1610.09736 (to appear in Medical Physics)*, 2016.
- [9] H. Chen, Y. Zhang, W. Zhang, P. Liao, K. Li, J. Zhou, and G. Wang, "Low-dose CT via convolutional neural network," *Biomedical optics express*, vol. 8, no. 2, pp. 679–694, 2017.
- [10] —, "Low-dose CT via convolutional neural network," *Biomedical optics express*, vol. 8, no. 2, pp. 679–694, 2017.
- [11] E. Kang and J. C. Ye, "Wavelet domain residual network (WavResNet) for low-dose X-ray CT reconstruction," in *2017 International Meeting on Fully Three-Dimensional Image Reconstruction in Radiology and Nuclear Medicine (arXiv preprint arXiv:1703.01383)*.
- [12] E. Kang, J. Yoo, and J. C. Ye, "Wavelet residual network for low-dose CT via deep convolutional framelets," *arXiv preprint arXiv:1707.09938*, 2017.
- [13] Y. Chen, W. Yu, and T. Pock, "On learning optimized reaction diffusion processes for effective image restoration," in *Proceedings of the IEEE Conference on Computer Vision and Pattern Recognition*, 2015, pp. 5261–5269.
- [14] X.-J. Mao, C. Shen, and Y.-B. Yang, "Image denoising using very deep fully convolutional encoder-decoder networks with symmetric skip connections," *arXiv preprint arXiv:1603.09056*, 2016.
- [15] J. Xie, L. Xu, and E. Chen, "Image denoising and inpainting with deep neural networks," in *Advances in Neural Information Processing Systems*, 2012, pp. 341–349.
- [16] K. H. Jin, M. T. McCann, E. Froustey, and M. Unser, "Deep convolutional neural network for inverse problems in imaging," *arXiv preprint arXiv:1611.03679*, 2016.
- [17] Y. Han, J. Yoo, and J. C. Ye, "Deep residual learning for compressed sensing CT reconstruction via persistent homology analysis," *arXiv preprint arXiv:1611.06391*, 2016.
- [18] J. C. Ye and Y. S. Han, "Deep convolutional framelets: A general deep learning for inverse problems," *arXiv preprint arXiv:1707.00372*, 2017.
- [19] R. Yin, T. Gao, Y. M. Lu, and I. Daubechies, "A tale of two bases: Local-nonlocal regularization on image patches with convolution framelets," *SIAM Journal on Imaging Sciences*, vol. 10, no. 2, pp. 711–750, 2017.
- [20] J. C. Ye, J. M. Kim, K. H. Jin, and K. Lee, "Compressive sampling using annihilating filter-based low-rank interpolation," *IEEE Transactions on Information Theory*, vol. 63, no. 2, pp. 777–801, Feb. 2017.
- [21] K. H. Jin and J. C. Ye, "Annihilating filter-based low-rank Hankel matrix approach for image inpainting," *IEEE Transactions on Image Processing*, vol. 24, no. 11, pp. 3498–3511, 2015.
- [22] K. H. Jin, D. Lee, and J. C. Ye, "A general framework for compressed sensing and parallel MRI using annihilating filter based low-rank hankel matrix," *IEEE Trans. on Computational Imaging*, vol. 2, no. 4, pp. 480–495, Dec 2016.
- [23] R. J. Duffin and A. C. Schaeffer, "A class of nonharmonic Fourier series," *Transactions of the American Mathematical Society*, vol. 72, no. 2, pp. 341–366, 1952.
- [24] S. Ioffe and C. Szegedy, "Batch normalization: Accelerating deep network training by reducing internal covariate shift," *arXiv preprint arXiv:1502.03167*, 2015.
- [25] A. Vedaldi and K. Lenc, "Matconvnet: Convolutional neural networks for matlab," in *Proceedings of the 23rd ACM international conference on Multimedia*. ACM, 2015, pp. 689–692.